Mechanism of CIT-6 and VPI-8 Crystallization from Zincosilicate Gels

David P. Serrano,*[a] Rafael van Grieken,[a] Mark E. Davis,[b] Juan A. Melero,[a] A. Garcia,[a] and G. Morales[a]

Abstract: The crystallisation of CIT-6, a large-pore zincosilicate with the framework topology of zeolite Beta and synthesised from clear hydrogels that contain, tetraethylammonium (TEA^+), Li^+ and Zn^{2+} cations, proceeds initially through the formation of an amorphous solid that incorporates all the initial Zn species. Nucleation of the *BEA phase is effected by reorganisation of the amorphous phase, whereas crystal growth involves the incorporation of soluble species also. A highly crystalline CIT-6 material is obtained after 164 h of synthesis at 140 °C. Scanning electron microscopy (SEM) shows that this sample exhibits two different types of crystals: well-defined pseudo-cubic crystals and rounded crystals. The latter has a broad crystal-size distribution. If crystallisation is continued with longer synthesis times, the VPI-8 crystalline phase appears, and a new population of needle-shaped crystals is detected in the SEM images. This new crystalline phase is nucleated on the surface of the rounded CIT-6 crystals, which disappear as the crystallisation progresses, while no changes are observed in the population of pseudo-cubic CIT-6 crystals. At higher crystallisation temperatures these phase transformations are accelerated, and the formation of VPI-8 is favoured over that of CIT-6.

Keywords: *BEA · CIT-6 · crystal growth · microporous materials · zeolites

Introduction

The synthesis of zeolite Beta (with *BEA topology) was first reported by Wadlinger et al.[1] The *BEA structure consists of an intergrowth of two polymorphs, denoted by A and B,[2] both of which contain winding 12-membered ring channels, cross-section 5.5 Å, along the *c* direction. These channels intersect with a set of straight 12-membered ring channels along the *a* and *b* directions with elliptical cross-sections of 6×7.3 and 6.8×7.3 Å for polymorphs A and B, respectively. This molecular sieve has been used successfully as a catalyst in hydrocarbon conversion processes[3] such as hydrocracking, dewaxing, fluid catalytic cracking, dealkylation, $C_8 - C_{10}$ separations and partial oxidation reactions.

The *BEA structure has been synthesised in the aluminosilicate form under different conditions,[4] most often with tetraethylammonium (TEA^+) as a structure-directing agent. Likewise, zeolite Beta isomorphously substituted by gallium,[5] boron,[6] iron[7] and titanium atoms[8] has been prepared. Zeolite Beta in its pure silica form has also been synthesised by various procedures.[9]

Davis et al. recently prepared a large-pore zincosilicate with the framework topology of zeolite Beta, named CIT-6.[10] This new material is synthesised under hydrothermal conditions from clear hydrogels containing Li^+ and Zn^{2+} cations and tetraethylammonium hydroxide (TEAOH). These studies showed that both Li^+ and Zn^{2+} cations are necessary for the formation of *BEA topology. Moreover, under particular conditions, such as long synthesis times, high temperatures and low TEAOH concentrations, the appearance of a new crystalline zincosilicate, VPI-8,[11] is observed in addition to the *BEA topology. VPI-8 has a 12-membered ring, a one-dimensional pore system and contains a novel "pinwheel" building unit in its structure.

In recent years it has been demonstrated that in many cases the crystallisation of zeolites is not just a solution-mediated process, but involves the participation of an X-ray-amorphous solid that undergoes solid–solid transformations with negligible incorporation of soluble species.[12] We report here a study of the different stages in the crystallisation of CIT-6 and the subsequent appearance of a VPI-8 phase.

Results and Discussion

To investigate the mechanism of CIT-6 synthesis from clear solutions containing Zn^{2+} and Li^+ cations, as well as the subsequent appearance of the VPI-8 phase, two series of

[a] Prof. D. P. Serrano, Prof. R. van Grieken, Prof. J. A. Melero, Prof. A. Garcia, Prof. G. Morales
Environmental and Chemical Engineering Group
School of Experimental Sciences and Technology
Rey Juan Carlos University, 28933 Mostoles, Madrid (Spain)
Fax: (+34) 91-664-74-90
E-mail: d.serrano@escet.urjc.es

[b] Prof. M. E. Davis
Chemical Engineering
California Institute of Technology
Pasadena, CA 91125 (USA)

  0947-6539/02/0822-5153 $ 20.00+.50/0

samples were prepared from crystallisations carried out with various synthesis times at 140 and 150 °C, respectively.

Synthesis conditions, overall crystallinity and the phases present in each sample are summarised in Table 1 and the X-ray diffraction (XRD) patterns and FT-IR spectra are illustrated in Figure 1 (S-1 to S-7). The solid collected after 70 h of synthesis (S-1) is amorphous as no diffraction peaks are observed in its XRD spectrum. Likewise, FT-IR bands in the range 450–750 cm^{-1}, which are typical of the zeolitic *BEA framework, are absent in this sample. The first signs of crystallinity appear in S-2 (prepared after 92 h of synthesis) with an XRD peak centred at $2\theta = 22.5°$ that corresponds with the major reflection of the *BEA topology. As the crystallisation progresses, the XRD peaks and the FT-IR skeleton vibrations at wavenumbers below 750 cm^{-1} increase in intensity. After 164 h of synthesis, a material (S-5) with very high crystallinity that exhibits the typical XRD pattern which corresponds to a pure *BEA structure is obtained. This sample was used as a reference for calculating the crystallinity and purity of the synthesised samples. Beyond that heating time, a VPI-8 phase is detected in the XRD spectra, its proportion increasing with the crystallisation time. Likewise, hydroxyl group concentration in the solid that is collected (FT-IR band centred at 3500 cm^{-1}) decreases in the first stages of the crystallisation, indicating an increase in the degree of condensation of silicon species.

Four steps can be distinguished in the TG-DTG curves of as-synthesised materials obtained at 140 °C with different synthesis times (Figure 2). The small weight loss produced below 100 °C accounts for the thermal desorption of water (step I). In the temperature range 100–200 °C (step II), the weight losses have been attributed to the decomposition of TEA^+ ions occluded within the amorphous solid phase, since this step is negligible for highly crystalline samples. A third step, ranging from 200 to 400 °C, is detected in the TG analysis. This weight loss is small for amorphous materials (S-1 and S-2) and becomes predominant for materials of higher crystallinity (S-3 to S-7). Hence, it probably originates from TEA^+ cations located within the zeolite cavities and pores. Finally, the broad weight loss observed between 400 and 700 °C (step IV) has been assigned in earlier work to the decomposition of TEA^+ residues strongly adsorbed on acid sites.[13] A reasonable estimate of the total TEA^+ content can be obtained from the overall weight loss associated with steps II, III and IV, whereas the TEA^+ cations present within a microporous crystalline network can be calculated from the

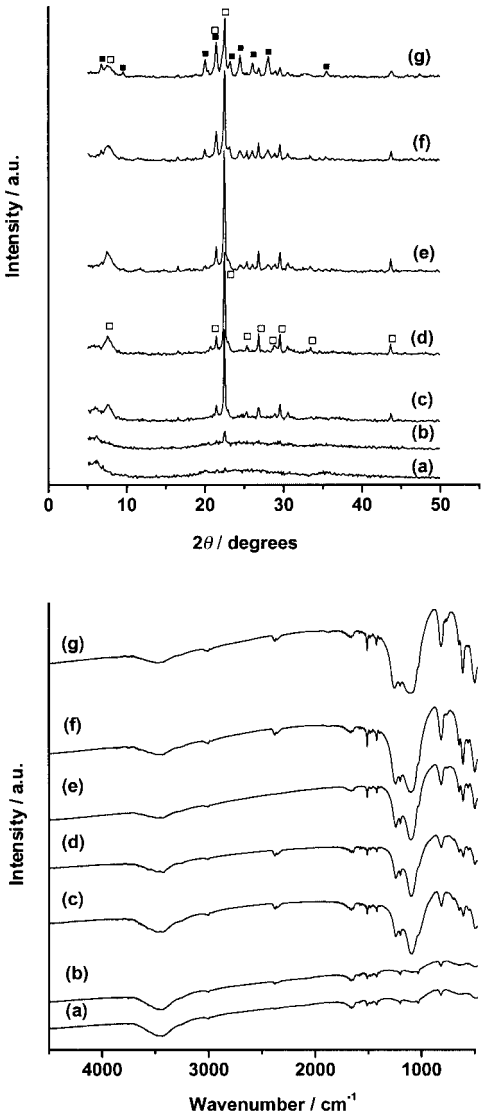

Figure 1. As-synthesised samples obtained at 140 °C for different crystallisation times: XRD patterns (top); FTIR spectra (bottom). Curves: a) S-1; b) S-2; c) S-3; d) S-4; e) S-5; f) S-6; g) S-7. (□) CIT-6 phase; (■) VPI-8 phase.

Table 1. Crystallisation kinetics of zincosilicate gels.

Sample	t_s [h][a]	T [°C]	Phases[b]	X_c[c] [%]	TGA[d] [%]	HCN[e] [%]
S-1	70	140	amorphous	0	37.9	32.0
S-2	92	140	amorphous + CIT-6	12	37.1	31.0
S-3	117	140	amorphous + CIT-6	75	22.8	20.3
S-4	137	140	amorphous + CIT-6	90	19.5	18.0
S-5	164	140	CIT-6	100	19.7	17.5
S-6	189	140	CIT-6 (75%) + VPI-8 (25%)	100	17.9	15.2
S-7	214	140	CIT-6 (49%) + VPI-8 (51%)	100	15.0	12.8
S-8	62	150	amorphous	0		
S-9	88	150	CIT-6 (41%) + VPI-8 (59%)	100		
S-10	98	150	CIT-6 (32%) + VPI-8 (68%)	100		
S-11	111	150	CIT-6 (23%) + VPI-8 (77%)	100		
S-12	136	150	CIT-6 (17%) + VPI-8 (83%)	100		

[a] Synthesis time. [b] Crystalline purity in brackets. [c] Crystallinity. [d] Weight loss assigned to peaks II, III and IV in TG analysis of as-synthesised samples. [e] HCN analysis of as-synthesised samples.

0947-6539/02/0822-5154 $ 20.00+.50/0 *Chem. Eur. J.* **2002**, *8*, No. 22

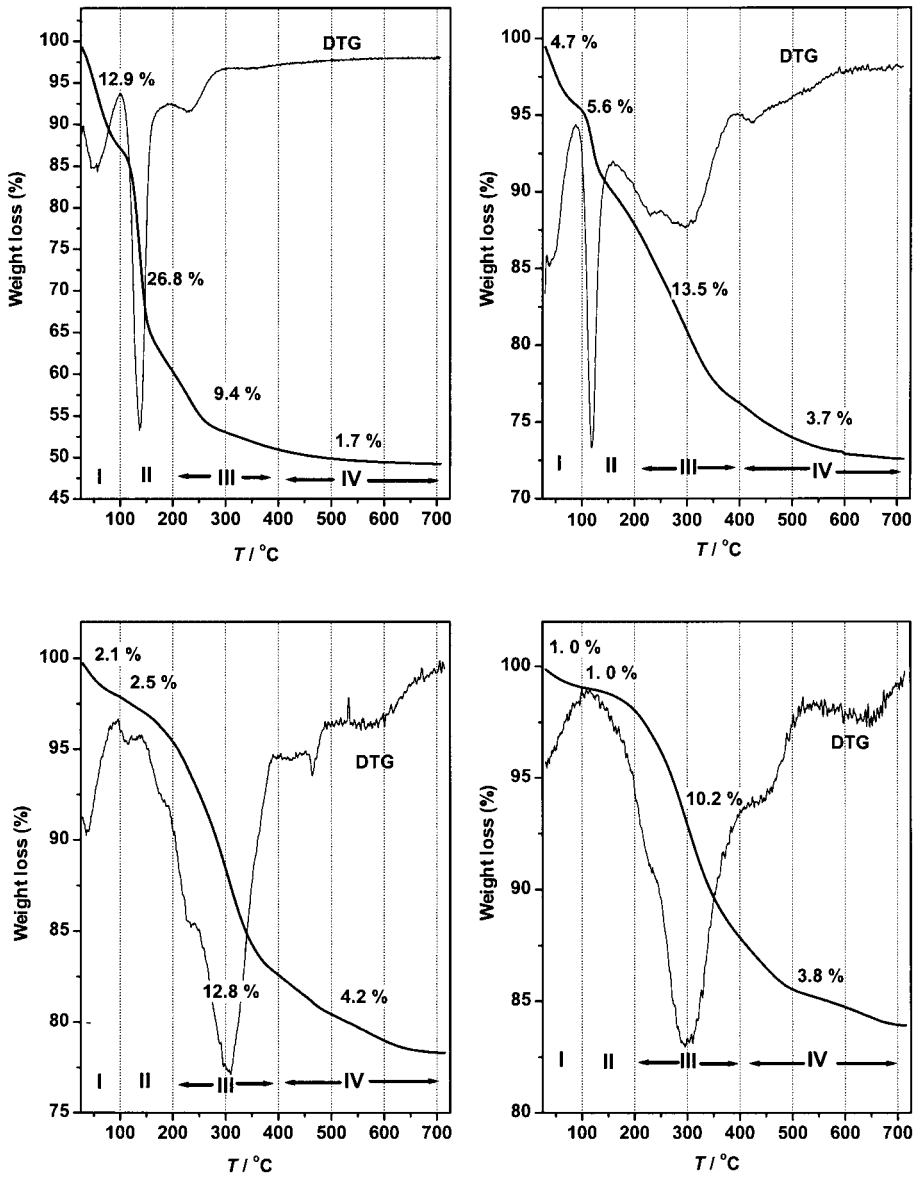

Figure 2. TG analyses of as-synthesised samples obtained at 140 °C for different crystallisation times: S-1 (top left); S-3 (top right); S-4 (bottom left); S-7 (bottom right).

weight loss associated with peaks III and IV. The HCN content of the as-synthesised samples in Table 1 is slightly lower than that assigned to the weight loss associated with steps II, III and IV. This difference, which is more accentuated in the amorphous materials, is probably due to the desorption of water at 100–200 °C (step II).

The gradual decrease in the total TEA^+ content incorporated into the samples with the crystallisation time (Table 1 and Figure 2) is a consequence of the transformation of the amorphous network into a microporous crystalline zeolitic material. The TEA^+ content of around 20 wt % estimated from the TG analysis for a highly crystalline *BEA material (S-5) is in fair agreement with the values reported in the literature for a pure *BEA-type zeolite,[4a] whereas the weight losses associated with steps III and IV decrease with the appearance of the VPI-8 phase and can be interpreted as a consequence of the lower microporosity present in this framework (0.10 $cm^3 g^{-1}$ for VPI-8;[11b] 0.21 $cm^3 g^{-1}$ for CIT-6). Furthermore, a gradual decrease in the content of adsorbed water (step I) is observed during the crystallisation, and indicates an enhancement in the hydrophobic character of the samples.

The evolution of crystallinity follows a typical sigmoid curve with an induction time of around 75 h for the detection of the first crystalline entities (Figure 3, top). This period is followed by a period with a high crystallisation rate, at which the crystallinity changes from 0 to 90 % in just 45 h. It is interesting that the amorphous solid obtained at short synthesis times is very rich in Zn^{2+} species; all the Zn^{2+} present initially in the synthesis gel is incorporated into the solid phase formed in the first stages of the crystallisation (Figure 3, top). Thus, S-2 contains all the Zn^{2+} species in the synthesis mixture in spite of having a crystallinity of just 12 %.

Crystallisation clearly evolves through three main steps (Figure 3, bottom). The first involves the formation of a white amorphous gel in which all Zn^{2+} species are completely incorporated. This step is followed by a gradual disappearance of the amorphous solid, which occurs simultaneously with the formation of the first CIT-6 crystals. The CIT-6 yield increases with the synthesis time to a maximum value around 60 % at 164 h. As mentioned earlier, the XRD pattern of this sample indicates it is a highly crystalline, pure CIT-6 phase. Thereafter, the VPI-8 phase appears, accompanied by an increase in the overall solid yield and a gradual decrease in the percentage of CIT-6.

The yield curves in Figure 3 (bottom) follow the classical pathway corresponding to series transformations, suggesting that CIT-6 zeolite is formed from the amorphous gel phase, while the VPI-8 crystallises from the CIT-6 phase. In line with this argument, all the Zn^{2+} species are incorporated into the solid phases from the earliest stages of the crystallisation; hence the solution phase consists of soluble silicates alone. The overall solid yield exhibits two plateaus that occur simultaneously with the appearance of the crystalline phases, and this suggests that the first steps in the formation of the CIT-6 and VPI-8 proceed directly from the pre-existing solid phase. However, both plateaus are followed by a significant

  0947-6539/02/0822-5155 $ 20.00+.50/0

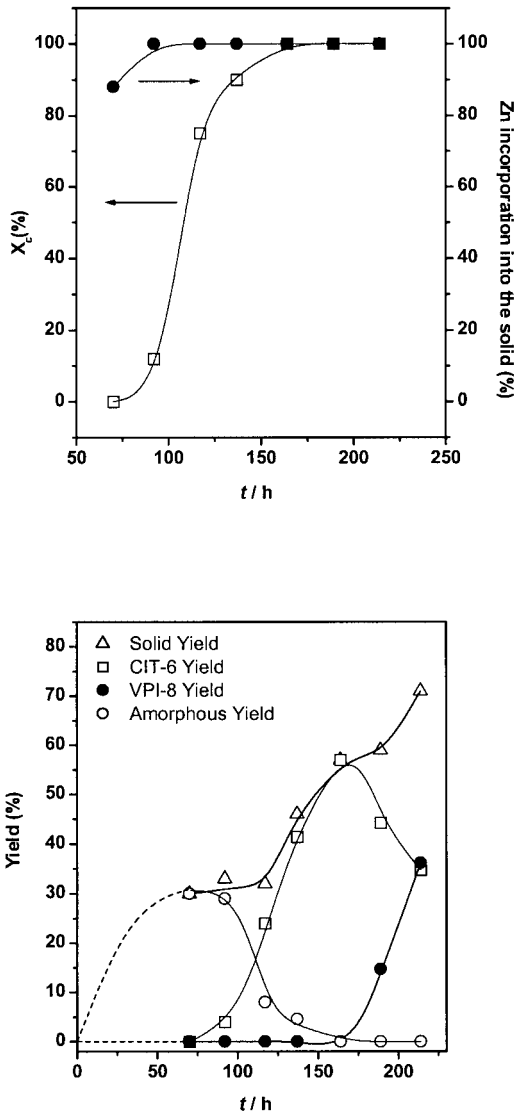

Figure 3. Top: Crystallisation kinetics and Zn^{2+} incorporation into the solid at 140 °C. Bottom: Evolution of the synthesis yield of the different solid phases with the crystallisation time.

increase in the overall solid, showing that the contribution of soluble silicate species is also significant (especially during the crystal growth steps). Thus, the silicon contents of the solids obtained, that is, $(Si/Zn)_{amorphous}$, $(Si/Zn)_{CIT-6}$ and $(Si/Zn)_{VPI-8}$, increase during the crystallisation process.

In good agreement with the amorphous nature predominant in the initial materials (S-1 to S-3), their ^{29}Si NMR spectra (Figure 4) exhibit three broad features associated with different Si connectivities:[14–15] $Q^3(1Zn)$ ($\delta = -93$), $Q^3(0Zn)$ ($\delta = -100$) and $Q^4(0Zn)$ ($\delta = -110$). The Q^3 species are associated with silanol groups, whereas the Q^4 originates from tetrahedrally coordinated Si atoms. Since both CIT-6 and VPI-8 molecular sieves are formed mainly by Si species with tetrahedral coordination, the decline observed with the synthesis time in the Q^3/Q^4 intensity ratio is a good indication of the progress of the crystallisation. The increase in the degree of condensation of the silicon species is in fair agreement with the decrease in the hydrophilic character of the samples during the crystallisation deduced from the TG

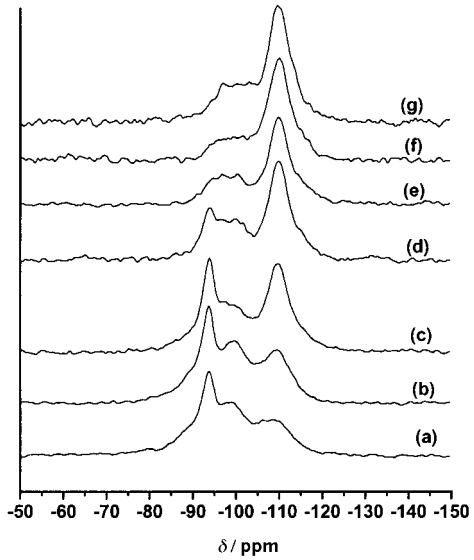

Figure 4. ^{29}Si MAS-NMR spectra of as-synthesised samples obtained at 140 °C: a) S-1; b) S-2; c) S-3; d) S-4; e) S-5; f) S-6; g) S-7.

analyses (above). However, the presence of the $Q^3(1Zn)$ resonance at $\delta = -93$ confirms that in the amorphous solid, formed in the earlier stages, the Zn^{2+} species are effectively incorporated into the silica matrix. As the synthesis time is increased, this resonance declines in intensity until it almost disappears for highly crystalline samples. Simultaneously, a small resonance appears, centred at $\delta = -95$. This band has been assigned to $Q^4(1Zn)$ species, indicating the presence of Si atoms connected to tetrahedrally coordinated Zn^{2+} atoms in the zeolitic framework.[14]

To follow the changes in the textural properties of the solid phases, N_2 adsorption/desorption isotherms at 77 K for calcined samples prepared at different synthesis times and their micropore volumes have been measured (Figure 5). The

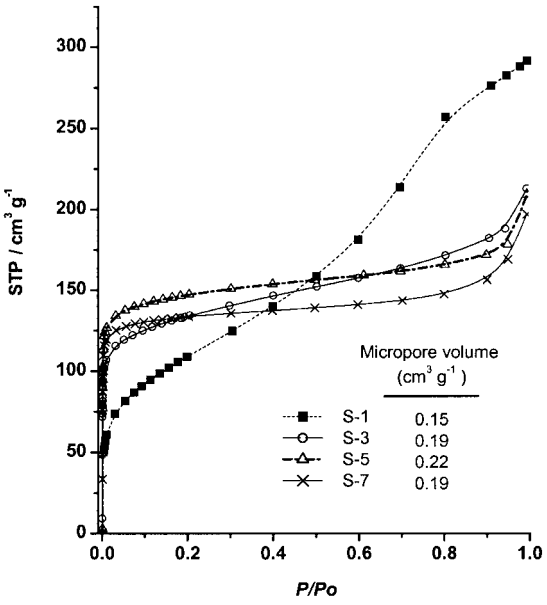

Figure 5. Nitrogen adsorption/desorption isotherms at 77 K of samples obtained at 140 °C for different synthesis times.

0947-6539/02/0822-5156 $ 20.00+.50/0 *Chem. Eur. J.* **2002**, *8*, No. 22

isotherm corresponding to the initial amorphous material (S-1) indicates that it exhibits both micro- and mesoporosity. The presence of a large volume of micropores in this amorphous material is remarkable; it suggests that the TEA^+ cations detected in this sample in the TG analysis may be located within the micropores before calcination. This initial amorphous material resembles the tetraethylammonium-containing microporous permutite reported by Di Renzo et al. as a synthesis intermediate of the zeolite Beta.[16] The isotherm corresponding to the material (S-3) obtained after 117 h of synthesis with a crystallinity of 75% represents a higher volume of micropores ($0.19\ cm^3 g^{-1}$). As the crystallisation progresses, a further increase in the microporosity to $0.22\ cm^3 g^{-1}$ for the pure CIT-6 material (S-5) is observed. The appearance of the VPI-8 phase (S-7) leads to a decrease in the overall micropore volume of the sample, which is in agreement with the lower microposity of this topology compared with CIT-6. For the amorphous materials, the pore size distribution in the mesopore range calculated using the Barrett–Joyner–Halenda (BJH) model (not shown in Figure 5) gives a maximum corresponding to a pore diameter of around 60 Å and this mesoporosity completely disappears as the crystallisation proceeds.

Figure 6 shows scanning electron microscopy (SEM) images of samples synthesised at 140 °C for different times: the amorphous solid initially formed (S-1; Figure 6a) is highly compact and dense, at least in the micrometer range. It is transformed into a particulate material as the CIT-6 phase is formed (S-3; Figure 6b), consisting of primary units with sizes below 0.5 μm. Taking into account the crystallinity of S-3 (75%), these primary units must be identified as CIT-6 crystals. However, most of them are present not as isolated particles, but as aggregates linked to the remaining amorphous solid phase. As the crystallisation progresses, larger particles arise from an aggregation process of the above-mentioned primary entities (S-4; Figure 6c). At this stage, although the VPI-8 phase has not been crystallised yet, the coexistence of two populations of CIT-6 crystals is detected: the first comprises crystals with well-defined pseudo-cubic morphology and sizes around 1 μm, whereas the second consists of crystals with a rounded shape and a broader particle size distribution. Both crystal types exhibit the *BEA topology, as concluded from the electron diffraction patterns obtained during transmission electron microscopy (TEM) measurements of the highly crystalline sample synthesised after 164 h of synthesis (S-5; Figure 7a).

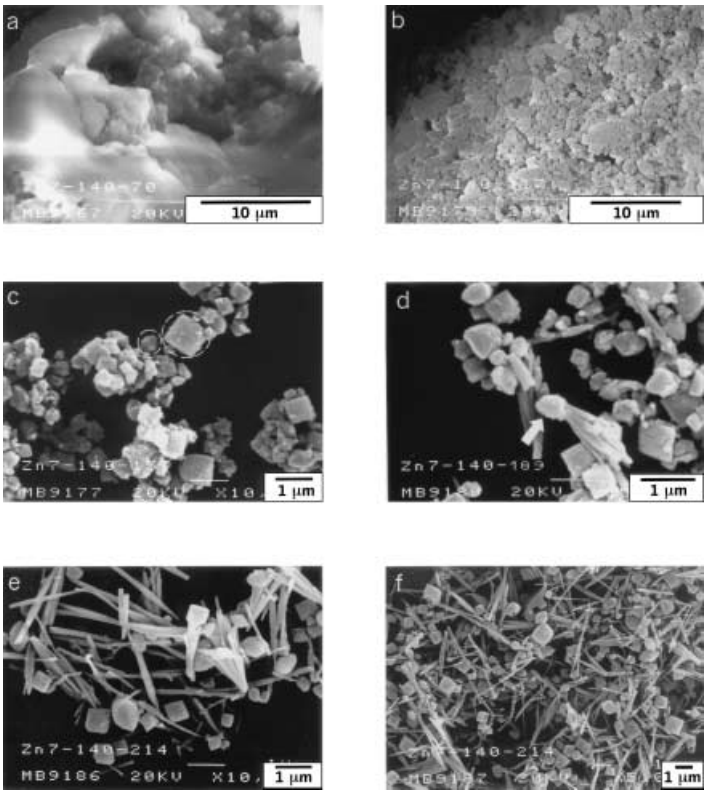

Figure 6. SEM images of as-synthesised samples obtained at 140 °C for different synthesis times: a) S-1; b) S-3; c) S-4; d) S-6; e) and f) S-7.

A further step in the crystallisation process leads to the appearance of needle-shaped crystals and corresponds to the formation of the VPI-8 phase (S-6; Figure 6d). Both SEM and TEM images (Figures 6d,e and 7b) show that the VPI-8 needle crystals are inserted and seem to emerge from the CIT-6 crystals, suggesting that the nucleation of the VPI-8 takes place on the Zn-containing CIT-6 crystals. This result is in agreement with a previous study postulating that the presence of Zn^{2+} cations is necessary for the VPI-8 phase to crystallise.[11a] In the system studied here, all the available Zn^{2+} has been incorporated first into the amorphous solid phase and subsequently into the CIT-6 crystals. Therefore, it is likely that the formation of VPI-8 crystals from nuclei generated in the liquid solution, free from Zn^{2+} species, does not occurr.

At longer synthesis times, SEM images show that the proportion of the VPI-8 needle crystals increases, whereas the rounded *BEA crystals are no longer detected (S-7; Figure 6e,f). Instead, most of the CIT-6 crystals observed in this sample present a pseudo-cubic morphology. These results can be interpreted by assuming that the rounded crystallites are not completely stable, and accordingly are converted into more stable pseudo-cubic crystals with the same topology or are consumed during the crystal growth of a VPI-8 phase with a different crystalline framework. This second alternative is supported by the decrease in the CIT-6 yield observed at long synthesis times, as the VPI-8 phase is formed (see Figure 3, bottom). Therefore both nucleation and the initial steps of crystal growth for VPI-8 proceed directly from CIT-6. The crystallisation process described in this work is a good example of Ostwald ripening in which thermodynamically favoured VPI-8 crystals grow at the expense of kinetically favoured CIT-6 crystals.[17]

To gain information about the effect of the temperature on the crystallisation of CIT-6 and VPI-8, a second kinetic run was carried out at a higher temperature (150 °C) starting from an initial mixture similar to that used in the previous experiment (S-8 to S-12; Table 1). Figure 8 (top) shows the XRD patterns of the as-synthesised samples obtained at different synthesis times. As at the lower temperature, an amorphous solid is detected before the formation of crystalline phases. The crystallisation at 150 °C is faster than at 140 °C, as indicated by the complete disappearance of the amorphous phase in just 25 h due to the formation of both

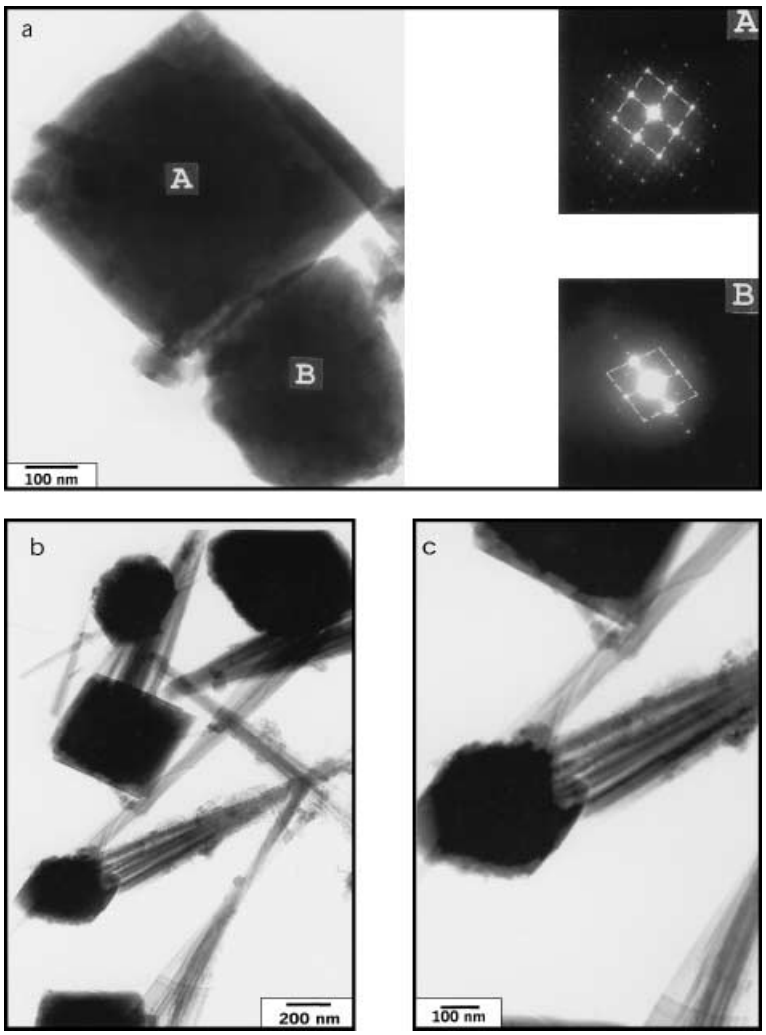

Figure 7. TEM images of as-synthesised samples obtained at 140 °C for different synthesis times: a) S-5; b) S-6; c) S-6 at higher resolution.

CIT-6 and VPI-8 materials. In contrast with the results obtained at the lower temperature, no pure crystalline *BEA phase is obtained: reflections assigned to both CIT-6 and VPI-8 crystalline phases are present in the XRD spectra of all samples. At longer synthesis times, a progressive increase in the XRD peaks corresponding to the VPI-8 phase is observed. These data indicate that at 150 °C the formation of the VPI-8 phase, instead of CIT-6, is favoured, and hence a pure *BEA phase cannot be obtained at this crystallisation temperature.

The changes in the yield of the different solid phases for the kinetic run at 150 °C in Figure 8 (bottom) show that, as at a lower temperature, an induction period is observed with the formation of an X-ray amorphous solid in a 55% yield; this solid incorporates all the Zn^{2+} species from the synthesis gel. However, the initial period is shortened significantly with the increase in temperature. This step is followed by a fast transformation of the amorphous solid into crystalline phases, which again incorporate all the Zn^{2+} species (as concluded from X-ray fluorescence (XRF) spectrometric analysis). In contrast with the crystallisation carried out at 140 °C, the transformation of the amorphous solid to yield CIT-6 crystals at 150 °C is accompanied by the simultaneous appearance of the VPI-8 phase. As at 140 °C, a significant decrease in the CIT-6 yield takes place during the last stage of the crystallisation and is accompanied by an increase in the percentage of VPI-8 phase. The proportion of VPI-8 in the final samples synthesised at 150 °C is substantially higher than that obtained at 140 °C.

The results obtained at the higher temperature are consistent with the conclusions stated above for the crystallisation mechanism: it comprises formation of an amorphous solid, crystallisation of CIT-6 zeolite and partial transformation of the latter into VPI-8. The major difference at 150 °C as opposed to 140 °C is that both crystalline phases are first detected simultaneously, and with a high proportion of VPI-8. This may be due to the fast transformation of CIT-6 into VPI-8 at that temperature, although the possible formation of VPI-8 directly from the amorphous solid should not be discounted.

Conclusion

Crystallisation mechanism: The following mechanism is proposed for the hydrothermal crystallisation of CIT-6 and VPI-8 zeolites from homogeneous hydrogels that contain TEA^+, Zn^{2+} and Li^+ cations under basic conditions (Figure 9). Initially, an amorphous solid, with a complete incorporation of Zn^{2+} species and a high content in TEA^+ species, is formed. Both the nucleation of the CIT-6 phase and the initial steps of crystal growth take place by reorganisation of this amorphous material. However, crystal growth also involves the incorporation of soluble species to yield two types of CIT-6 crystals with complete incorporation of the Zn^{2+} species: small rounded crystals with a wide size distribution and a second population of well-defined pseudo-cubic crystals (pathway I). In a further step, the nucleation and the initial crystal growth of the VPI-8 phase occurs on the *BEA particles, in particular on those crystals with a rounded shape (pathway II). A decrease in the CIT-6 yield is observed at long synthesis times as a consequence of its partial conversion into VPI-8. The reaction temperature plays an important role in the various transformations involved in the crystallisation process. At a higher temperature, the crystallisation kinetics are accelerated, with a faster reorganisation of the amorphous solid to yield both crystalline phases (pathways I and III), as well as with a faster transformation of CIT-6 crystals into the VPI-8 phase (pathway II).

0947-6539/02/0822-5158 $ 20.00+.50/0 *Chem. Eur. J.* **2002**, *8*, No. 22

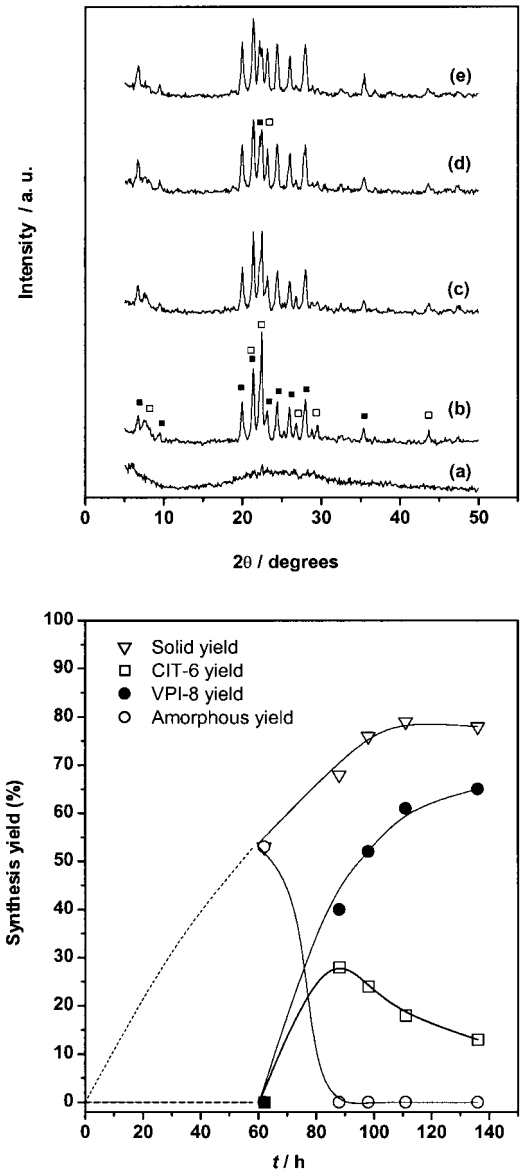

Figure 8. The different solid phases obtained at 150 °C for different crystallisation times: XRD pattern (top); synthesis yields (bottom). Curves: a) S-8; b) S-9; c) S-10; d) S-11; e) S-12. (□) CIT-6 phase (■) VPI-8 phase.

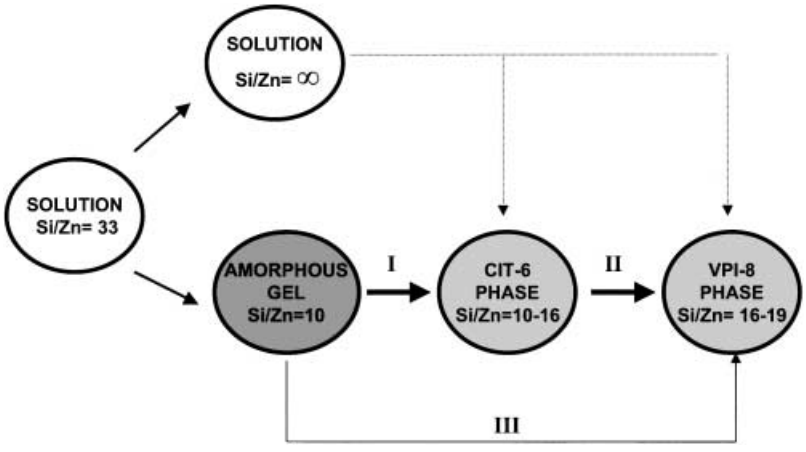

Figure 9. Proposed mechanism for the CIT-6 and VPI-8 crystallisation.

Experimental Section

Sample preparation: The chemical reagents used and the sources were tetraethylammonium hydroxide (TEAOH, 35 wt % aqueous solution, Aldrich), colloidal silica (Ludox AS-40, Dupont), zinc acetate dihydrate (Aldrich) and lithium hydroxide monohydrate (Aldrich). The starting hydrogel was prepared as follows: an aqueous solution containing the inorganic (Zn^{2+}, 2.50 mmol; Li^{+}, 4.17 mmol) and organic (TEA^{+}, 54 mmol) cations was stirred until the inorganic salts had dissolved completely. Thereafter, the silicon source (12.5 g, 83 mmol of Si) was added dropwise, and the resulting mixture was stirred for 3 h at 80 °C under reflux to obtain a clear solution. The reaction mixture (molar composition $1\,SiO_2$:0.03 $ZnAc_2\cdot 2\,H_2O$:0.05 LiOH – H_20:0.65 TEAOH:30 H_2O) was loaded into several Teflon-lined autoclaves and crystallised by thermal treatment under autogenous pressure and static conditions at various temperatures (140 – 150 °C) and synthesis times. The solid synthesis products were recovered by centrifugation, washed several times with distilled water and dried overnight at 110 °C. The solid synthesis yield (Y_s) was calculated as the weight of solid obtained once the template had been removed by calcination, as a percentage of the weight of SiO_2 in the initial mixture.

Characterisation: XRF chemical analyses were performed with a Philips PW1480 spectrometer, and HCN analyses in an Exeter Analytical apparatus. XRD patterns were collected with a Philips X'Pert diffractometer with $Cu_{K\alpha}$ radiation. For partially crystalline *BEA samples, the crystallinity (X_c) was determined by comparison of the intensity of the peak located at $2\theta = 22.5°$ with that of the sample obtained after 164 h, considered as 100 % crystalline (adsorption volume consistent with a highly crystalline sample of *BEA topology). The amorphous yield was estimated from the overall solid yield Y_s and the crystallinity of the sample X_c [%] according to Equation (1).

$$Y_{\text{amorphous}} = Y_s\left[1 - \frac{X_c}{100}\right] \quad (1)$$

For 100 % crystalline samples consisting of a mixture of CIT-6 and VPI-8, the proportion of the *BEA phase was estimated by comparison of the intensity of the peak located at $2\theta = 22.5°$ (I_{sample}) with that of the sample obtained after 164 h (I_{164}), considered as pure CIT-6 crystalline material. Thereby Equations (2) and (3) were used to determine the percentage of each crystalline phase.

$$\text{Phase}_{\text{CIT-6}}\,[\%] = 100 \times \frac{I_{\text{sample}}}{I_{164}} \quad (2)$$

$$\text{Phase}_{\text{VPI-8}}\,[\%] = 100 - \text{Phase}_{\text{CIT-6}}\,[\%] \quad (3)$$

Consequently, the synthesis yields corresponding to the CIT-6 and VPI-8 phases for 100 % crystalline samples were defined by Equations (4) and (5).

$$Y_{\text{CIT-6}} = Y_s\left[\frac{\%\,\text{Phase}_{\text{CIT-6}}}{100}\right] \quad (4)$$

$$Y_{\text{VPI-8}} = Y_s - Y_{\text{CIT-6}} \quad (5)$$

FT-IR spectra were recorded on a Nicolet 510P spectrophotometer using the KBr wafer technique. An EXSTAR 6000 thermogravimetric analyser was used for simultaneous thermal analysis combining thermogravimetry (TG) and difference thermogravimetry (DTG) with a heating rate of 10 °C min^{-1} in an air atmosphere.

^{29}Si magic-angle spinning nuclear magnetic resonance (MAS-NMR) spectra of powdered samples were recorded at 59.57 MHz on a Varian VXR-300 spectrometer. The spinning frequency was 4 kHz and intervals ranging from 5 to 30 s between successive accumulations were selected according to the crystallinity of the samples. The meas-

urements were carried out at room temperature with tetramethylsilane (TMS) as external standard reference and with accumulations amounting to 2000.

Nitrogen isotherms at 77 K were determined using a volumetric adsorption apparatus (Micromeritics, ASAP 2010). Pore size distribution in the mesopore range was obtained by applying the BJH model with cylindrical geometry of the pores and by using the Harkins and Jura equation for determining the adsorbed layer thickness. The morphology and size of the crystals were determined by scanning electron microscopy (SEM) with a JEOL JSM-6400 microscope and transmission electron microscopy (TEM) with a JEOL JEM-200 FX microscope.

Acknowledgement

We are grateful for the financial support from Comunidad de Madrid throughout the "Grupos Estratégicos" project.

[1] R. L. Wadlinger, G. T. Kerr, E. J. Rosinski, US 3308069, **1967**.
[2] J. B. Higgins, R. B. La Pierre, J. L. Schlenker, A. C. Rohrman, J. D. Wood, G. T. Kerr, W. J. Rohrbaugh, *Zeolites* **1988**, *5*, 446 – 452.
[3] M. E. Davis, S. I. Zones, in *Synthesis of Porous Materials: Zeolite Clays and Nanostructures* (Eds: M. L. Occelli, H. Kessler), Dekker, New York, **1996**.
[4] a) J. Perez-Pariente, J. A. Martens, P. A. Jacobs, *Zeolites* **1988**, *8*, 46 – 53; b) M. A. Camblor, J. Perez-Pariente, *Zeolites* **1991**, *11*, 202 – 210; c) M. A. Camblor, A. Mifsud, J. Perez-Pariente, *Zeolites* **1991**, *11*, 792 – 797; d) R. B. Borade, A. Clearfield, *Catal. Lett*. **1994**, *26*, 285 – 289; e) R. B. Borade, A. Clearfield, *Microporous Mater*. **1996**, *5*, 289 – 297; f) P. R. H. P. Rao, M. Matsukata, *Chem. Commun*. **1996**, 1441 – 1442; g) M. A. Camblor, A. Corma, S. Valencia, *J. Mater. Chem.* **1998**, *8*, 2137 – 2145; h) M. A. Camblor, A. Corma, S. Valencia, *Microporous Mesoporous Mater.* **1998**, *25*, 59 – 74.
[5] a) M. A. Camblor, J. Perez-Pariente, V. Fornes, *Zeolites* **1992**, *12*, 280 – 286; b) S. G. Hedge, R. A. Abdullah, R. N. Bhat, P. Ratnasamy, *Zeolites* **1992**, *12*, 951 – 956; c) M. L. Ocelli, H. Eckert, A. Wolker, A. Auroux, *Microporous Mesoporous Mater.* **1999**, *30*, 219 – 232.
[6] a) R. Deruiter, K. Pamin, A. P. M. Kentgens, J. C. Jansen, H. van Bekkum, *Zeolites* **1993**, *13*, 611 – 621; b) J. C. van der Waal, M. S. Rigutto, H. van Bekkum, *J. Chem. Soc. Chem. Commun*. **1994**, 1241 – 1242; c) S. Kallus, J. Patarin, P. Caullet, A. C. Faust, *Microporous Mater*. **1997**, *10*, 181 – 188.
[7] a) R. Kumar, A. Thangaraj, R. N. Bhat, P. Ratnasamy, *Zeolites* **1990**, *10*, 85 – 89; b) R. Kumar, S. K. Date, E. Bill, A. Trautwein, *Zeolites* **1991**, *11*, 211 – 213; c) P. N. Joshi, E. M. Joseph, V. P. Shiralkar, *J. Chem. Soc. Chem. Commun*. **1994**, 387 – 393.
[8] a) M. A. Camblor, A. Corma, A. Martinez, J.Perez-Pariente, *J. Chem. Soc. Chem. Commun.* **1992**, 589 – 590; b) M. A. Camblor, M. Constantini, A. Corma, P. Esteve, L. Gilbert, A. Martinez, S. Valencia, *Appl. Catal*. **1995**, *133*, 185 – 189; c) J. S. Reddy, A. Sayari, *J. Chem. Soc. Chem. Commun.* **1995**, 23 – 24; d) T. Blasco, M. A. Camblor, A. Corma, P.Esteve, A.Martinez, C. Prieto, S. Valencia, *Chem. Commun*. **1996**, 2367 – 2368; e) J. C. van der Waal, P. J. Kooyman, J. C. Jansen, H. van Bekkum, *Microporous Mesoporous Mater.* **1998**, *25*, 43 – 57; f) D. P. Serrano, M. A. Uguina, G. Ovejero, R. van Grieken, M. Camacho, J. A. Melero, *J. Mater. Chem*. **1999**, *9*, 2899 – 2905.
[9] a) M. A. Camblor, A. Corma, S. Valencia, *Chem. Commun*. **1996**, 2365 – 2366; b) M. A. Camblor, L. A. Villaescusa, M. J. Diaz-Cabanas, *Top. Catal.* **1999**, *9*, 59 – 76.
[10] a) T. Takewaki, L. W. Beck, M. E. Davis, *J. Phys. Chem. B* **1999**, *103*, 2674 – 2679; b) T. Takewaki, L. W. Beck, M. E. Davis, *Top. Catal*. **1999**, *9*, 35 – 42.
[11] a) M. Yoshikawa, S. I. Zones, M. E. Davis, *Microporous Mater*. **1997**, *11*, 127 – 136; b) M. Yoshikawa, S. I. Zones, M. E. Davis, *Microporous Mater*. **1997**, *11*, 137 – 148.
[12] a) C. E. A. Kirschhock, R. Ravishankar, P. A. Jacobs, J. A. Martens, *J. Phys. Chem. B* **1999**, 103, 11021 – 11027; b) P. P. E. A. de Moor, T. P. M. Beelen, R. A. van Santen, L. W. Beck, M. E. Davis, *J. Phys. Chem. B* **2000**, 104, 7600 – 7611; c) J. A. Melero, R. van Grieken, D. P. Serrano, J. J. Espada, *J. Mater. Chem*. **2001**, 11, 1519 – 1525; d) D. P. Serrano, R. van Grieken, *J. Mater. Chem*. **2001**, *11*, 2391 – 2407.
[13] V. Kanazirev, G. L. Price, *J. Catal.* **1996**, *161*, 156 – 163.
[14] M. A. Camblor, M. E. Davis, *J. Phys. Chem. B* **1994**, *98*, 13151 – 13156.
[15] G. Engelhardt, D. Michel, *High Resolution Solid-State NMR of Silicates and Zeolites*, Wiley, Chichester, **1987**, p. 147.
[16] M. A. Nicolle, F. Di Renzo, F. Fajula, P. Espiau, T. Des Courieres, in *Proceedings of the 9th International Zeolite Conference* (Eds.: R. Von Ballmoos, J. B. Higgins, M. M. J. Treacy), Butterworth – Heinemann, Boston, **1993**, pp. 313 – 320.
[17] a) R. Boistelle, J. P. Astier, *Cryst. Growth* **1988**, *90*, 14 – 30; b) S. I. Zones, S. J. Hwang, M. E. Davis, *Chem. Eur. J.* **2001**, *7*, 1990 – 2001; c) R. Szostack, *Molecular Sieves, Principles of Synthesis and Identificatio*n, Van Nostrand Reinhold, New York, **1989**, p. 53.

Received: March 27, 2002 [F3978]

  0947-6539/02/0822-5160 $ 20.00+.50/0